A comparison between head-on quenching of stoichiometric methane-air and hydrogen-air premixed flames using Direct Numerical Simulations

Jiawei Lai[1], Umair Ahmed[2], Markus Klein[3, *], Nilanjan Chakraborty[2]

[1]CMCL Innovations, Cambridge, CB3 0AX, UK

[2]School of Engineering, Newcastle University, Newcastle-Upon-Tyne, NE1 7RU, UK

[3]Universität der Bundeswehr München, Fakultät für Luft- und Raumfahrttechnik

Email: markus.klein@unibw.de

ABSTRACT

Head-on quenching of statistically planar stoichiometric methane-air and hydrogen-air flames has been compared based on a Direct Numerical Simulation (DNS) database. Due the absence of OH at the wall CO cannot be oxidised anymore which leads to the accumulation of carbon monoxide in the near-wall region during flame quenching of stoichiometric methane-air flames. Furthermore, for both fuels, low-temperature reactions at the wall have been found to give rise to accumulation of HO_2 and H_2O_2 during flame quenching. As a result of this, a non-zero heat release rate can be observed at the wall during flame-wall interaction and this effect is particularly strong for the head-on quenching of the stoichiometric hydrogen-air premixed flame. The minimum Peclet number (i.e. normalised flame quenching distance) and the normalised wall heat flux magnitude are found to be smaller in the stoichiometric hydrogen-air flame than in the stoichiometric methane-air premixed flame. Moreover, it has been found that the flame quenching distance tends to decrease under turbulent conditions for the head-on quenching of the stoichiometric hydrogen-air premixed flame but the quenching distances for laminar and turbulent conditions remain comparable for the stoichiometric methane-air premixed flame. The mean reaction rate of reaction progress variable is not properly predicted in the near-wall region by well-known closures for the Flame Surface Density (FSD) or scalar dissipation rate (SDR). For FSD based mean reaction rate closure, it has been observed that recently proposed, simple chemistry DNS based, near-wall corrections perform satisfactorily for both fuels for the detailed chemistry case without adjustment of the model parameters. However, the previously proposed near-wall modification to an algebraic SDR closure based on simple chemistry data performs satisfactorily for the head-on quenching of stoichiometric methane-air premixed flame but it is found to be less effective in the case of the head-on quenching of stoichiometric hydrogen-air premixed flame. Moreover, the prediction of the mean heat release rate for head-on quenching of the stoichiometric hydrogen-air premixed flame cannot be achieved by the mean reaction rate closure of the reaction progress variable based on the mass fraction of a major species because of the important role played by intermediate species in the heat release rate at the wall.

Keywords: Flame-wall interaction, head-on quenching, Direct Numerical Simulation, wall heat flux, Peclet number, stoichiometric methane-air premixed flame, stoichiometric hydrogen-air premixed flame

1. INTRODUCTION

Modern combustors are often made smaller in size to increase energy-density and to adapt them for future electric powertrains. For small-sized combustors, the flame elements interact with the wall and alter the flow dynamics close to the wall, which will in turn affect the flame and chemical reactions in the vicinity of the wall. The flame-wall interaction determines the heat transfer through the wall, efficiency loss due to flame quenching and unburned fuel emission. Thus, a thorough understanding of the physics of the flame behaviour in the near-wall region is urgently needed. In this respect, a configuration, which is commonly known as the head-on quenching (Poinsot et al., 1993; Poinsot and Veynante, 2001), can present an ideal testbed where the mean direction of flame propagation aligns with the wall-normal direction and the flame quenches as it comes in the vicinity of a cold isothermal wall due to the heat loss through the wall. Poinsot et al. (1993) carried out two-dimensional Direct Numerical Simulations (DNS) to analyse the maximum heat flux and the flame quenching distance along with near-wall flame dynamics based on a single-step Arrhenius-type irreversible chemical reaction. The findings by two-dimensional simple chemistry DNS of head-on quenching have been found to be in good qualitative agreement with two-dimensional detailed chemistry simulations of head-on quenching of H_2 − air premixed flames by Dabireau et al. (2003). It has recently been demonstrated by Lai and Chakraborty (2016a,b) using simple chemistry DNS of head-on quenching of turbulent premixed flames that the findings in terms of wall heat flux and flame quenching distance from two-dimensional simulations (Poinsot et al., 1993) remain both qualitatively and quantitatively valid even for three-dimensional turbulent flow conditions. Lai et al. (2018) subsequently analysed the head-on quenching of both laminar and turbulent statistically planar CH_4 − air premixed flames by an isothermal inert wall based on both single-step and skeletal multi-step chemical mechanisms and revealed that the maximum wall heat flux and the flame quenching distance are not affected by the choice of the chemical mechanism. It was demonstrated by Lai et al. (2018) that the head-on quenching of premixed flames is principally driven by heat transfer and not by the choice of chemical mechanism (Lai et al., 2018). However, it has been found that both heat release rate and reaction rate of progress variable based on fuel mass fraction vanish at the wall for simple chemistry simulations, but the heat release rate does not vanish at the wall for the detailed chemistry simulations due to low-temperature chemistry involving

HO_2 and H_2O_2 (Lai et al., 2018). Moreover, the absence of OH in the near-wall region leads to a high concentration of CO in the vicinity of the cold wall (Lai et al., 2018), which is consistent with previous experimental findings (Mann et al., 2014; Jainski et al., 2017a,b; Kosaka et al., 2020). The CO production in the near-wall region was subsequently confirmed based on unsteady two-dimensional head-on quenching simulation (Palulli et al., 2019; Jiang et al., 2019) and three-dimensional DNS of sidewall quenching of turbulent V-flames (Jiang et al., 2021). Despite these differences between simple and detailed chemistry simulations, the models for the Flame Surface Density (FSD)/Scalar Dissipation Rate (SDR), that have been developed based on simple chemistry DNS data (Lai et al., 2016a,b; Sellmann et al., 2017), have also been found to be valid based on detailed chemistry simulations (Lai et al., 2018) and experimental (Jainski et al., 2017a) data.

Hydrogen is becoming increasingly popular as an alternative fuel for the future (Strategic framework for hydrogen energy in the UK, 2004) and thus it is important to compare and contrast the flame-wall interaction for hydrogen-air flames with that for conventional hydrocarbon-air (e.g. methane-air) flames under statistically similar conditions so that the differences in behaviours can be utilised to design future generation combustors to be operated based on high hydrogen content fuels. However, a comparison of flame-wall interactions for H_2-air and hydrocarbon-air flames under statistically similar conditions is rarely found in the existing literature. The present paper will address this void in the existing literature by carrying out three-dimensional detailed chemistry Direct Numerical Simulations (DNS) of head-on quenching of statistically planar flames for stoichiometric H_2 −air and CH_4 −air mixtures for identical values of normalised turbulence intensity u'/S_L and integral length scale to flame thickness ratio l/δ_{th} away from the wall, where u' is the root-mean-square value of velocity, S_L is the unstrained laminar burning velocity, l is the integral length scale of turbulence and $\delta_{th} = (T_{ad} - T_0)/\max|\nabla T|_L$ is the thermal flame thickness with T, T_0 and T_{ad} being the instantaneous, unburned gas and adiabatic flame temperatures, respectively. The DNS data has been utilised to compare the near-wall flame dynamics between head-on quenching of both laminar and turbulent statistically planar stoichiometric premixed H_2 − air and CH_4 − air premixed flames by an inert cold wall. In this respect, the main objectives of this analysis are:

(a) To compare the spatial distributions of species mass fractions, temperature, heat release rate, and the magnitudes of maximum heat flux and the minimum Peclet number for stoichiometric $CH_4 -$ air and $H_2 -$ air premixed flames under both laminar and turbulent conditions with identical values of turbulence intensity and integral length scale to flame thickness ratio.

(b) To assess if the near-wall modelling of the mean reaction rate and FSD/SDR closure in the case of head-on quenching of stoichiometric $H_2 -$ air premixed flames can be achieved similarly as that in the case of stoichiometric $CH_4 -$ air premixed flames.

The aforementioned aspects will be discussed thoroughly in section 3 after introducing the mathematical and physical formulation in section 2. Finally, the main conclusions will be summarised in the final section of this paper.

2. GOVERNING EQUATIONS AND NUMERICAL IMPLEMENTATION

The well-known, compressible SENGA2 code (Cant, 2012) has been employed to perform the detailed chemistry, three-dimensional, turbulent HOQ DNS. A resolution of 15 grid points across the thermal flame thickness δ_{th} results in a uniform Cartesian grid of dimension $256 \times 256 \times 256$ for a cubic domain with a side length of 7.65 mm. High order spatial (10^{th} order central difference scheme for the internal grid points decreasing at non-periodic boundaries to a one-sided 4^{th} order scheme) and temporal discretization schemes (explicit low-storage 4^{th} order Runge-Kutta) guarantee an accurate solution of the governing equations. The mean flame propagation takes place in the negative x_1-direction. The inert, isothermal wall at the left-hand boundary is kept at an unburned gas temperature T_0 of 300 K, while the opposite wall is taken to be partially non-reflecting (Poinsot and Lele, 1992). The directions perpendicular to the direction of mean flame propagation are taken to be periodic. A no-slip condition is imposed on the wall, which is considered to be isothermal, and the wall-normal diffusive flux is taken to be zero. The methane-air chemistry has been described by a skeletal chemical mechanism for atmospheric pressure combustion involving 16 species and 25 reactions (among these 10 reactions are reversible) (Smooke and Giovangigli, 1991). By contrast, a chemical mechanism involving 9 species and 19 reactions (Li et al., 2004) has been used for simulations of H_2-air premixed flames. CHEMKIN (Kee et al., 2000) polynomials have been used to specify the temperature dependent thermo-physical

properties, such as viscosity or thermal conductivity. Mixture-averaged transport is adopted for both CH_4-air and H_2-air premixed flame simulations. The reacting species and temperature fields have been initialised using a 1D steady-state solution for the appropriate stoichiometry and thermochemistry. The turbulent fluctuations away from the wall have been generated using a synthetic, homogeneous isotropic velocity field following Rogallo (1981). No slip conditions are specified for all velocity components at the wall and the diffusive mass fluxes in the wall normal direction are considered to be zero. Table 1 summarises the initial turbulence parameters away from the wall for cases A and B: the initial values of normalised root-mean-square (rms) turbulent velocity fluctuation u'/S_L, the ratio of integral length scale to flame thickness l/δ_{th}, the Damköhler and Karlovitz numbers $\mathrm{Da} = lS_L/u'\delta_{th}$, and $\mathrm{Ka} = (u'/S_L)^{1.5}(l/\delta_{th})^{-0.5}$ along with the heat release parameter values $\tau = (T_{ad} - T_0)/T_0$.

Table 1. Initial turbulence parameters away from the wall

Case	Mixture	Chemical Mechanism	u'/S_L	l/δ_{th}	Da	Ka	τ
A	Stoichiometric $H_2 - $ air	9 species, 19 reactions	5.0	2.5	0.5	7.0	7.0
B	Stoichiometric $CH_4 - $ air	16 species, 25 reactions	5.0	2.5	0.5	7.0	6.0

The simulations have been run for 18 initial eddy turnover times (i.e. $18\, l/u'$) for cases A and B to ensure that the maximum and the minimum wall heat fluxes approach each other. In all simulations it has been ensured that the dimensionless wall normal distance $x^+ = u_\tau \Delta x/\nu$ remains smaller than unity at all times (here $u_\tau = \sqrt{|\tau_w|/\bar{\rho}}$ is the friction velocity, Δx is the grid spacing, ν, τ_w and $\bar{\rho}$ are the kinematic viscosity the mean wall shear stress and mean gas density at the wall, respectively). Both cases A and B fall on the same location on the Borghi-Peters diagram (Peters 2000) and they nominally represent the thin reaction zones regime combustion (Peters, 2000). The adiabatic flame temperature for the stoichiometric $CH_4 - $ air mixture is different to the stoichiometric $H_2 - $ air flame for the same unburned gas temperature (i.e. $T_0 = 300$ K), and thus the values of heat release parameter $\tau = (T_{ad} - T_0)/T_0$ for cases A and B are different. However, this difference in τ values should not play a major role because it was demonstrated previously (Poinsot et al., 1993; Poinsot and Veynante, 2001) that the

heat flux and the flame quenching distance in the case of head-on quenching are not significantly affected by the heat release parameter.

The reaction progress in premixed flames, can be quantified either in terms of the reaction progress variable c or using non-dimensional temperature T as follows (Poinsot et al., 1993; Poinsot and Veynante, 2001)

$$c = \frac{Y_{\mathrm{R},0} - Y_{\mathrm{R}}}{Y_{\mathrm{R},0} - Y_{\mathrm{R},\infty}} \quad \text{and} \quad T = \frac{\hat{T} - T_0}{T_{\mathrm{ad}} - T_0} \, . \tag{1}$$

Here the subscripts 0 and ∞ indicate values in the unburned and fully burned gas respectively and Y_{R} denotes a suitable reactant mass fraction. This convention results in a value of $c = 0.0$ in the unburned reactants and $c = 1.0$ in the fully burned products and increases monotonously in between. The reaction progress variable c is defined based on methane and hydrogen mass fractions, for cases A and B respectively. It is also worth noting that alternative definitions of c are possible by using either an alternative reactant mass fraction (e.g. O_2 mass fraction) in Eq. 1 or by using a suitable product mass fraction Y_{P} (e.g. H_2O mass fraction) in $c = (Y_{\mathrm{P}} - Y_{\mathrm{P},0})/(Y_{\mathrm{P},\infty} - Y_{\mathrm{P},0})$. The choice of the definition of c does not directly affect the conclusions of the analysis conducted here, and thus this aspect will not be discussed further in this paper.

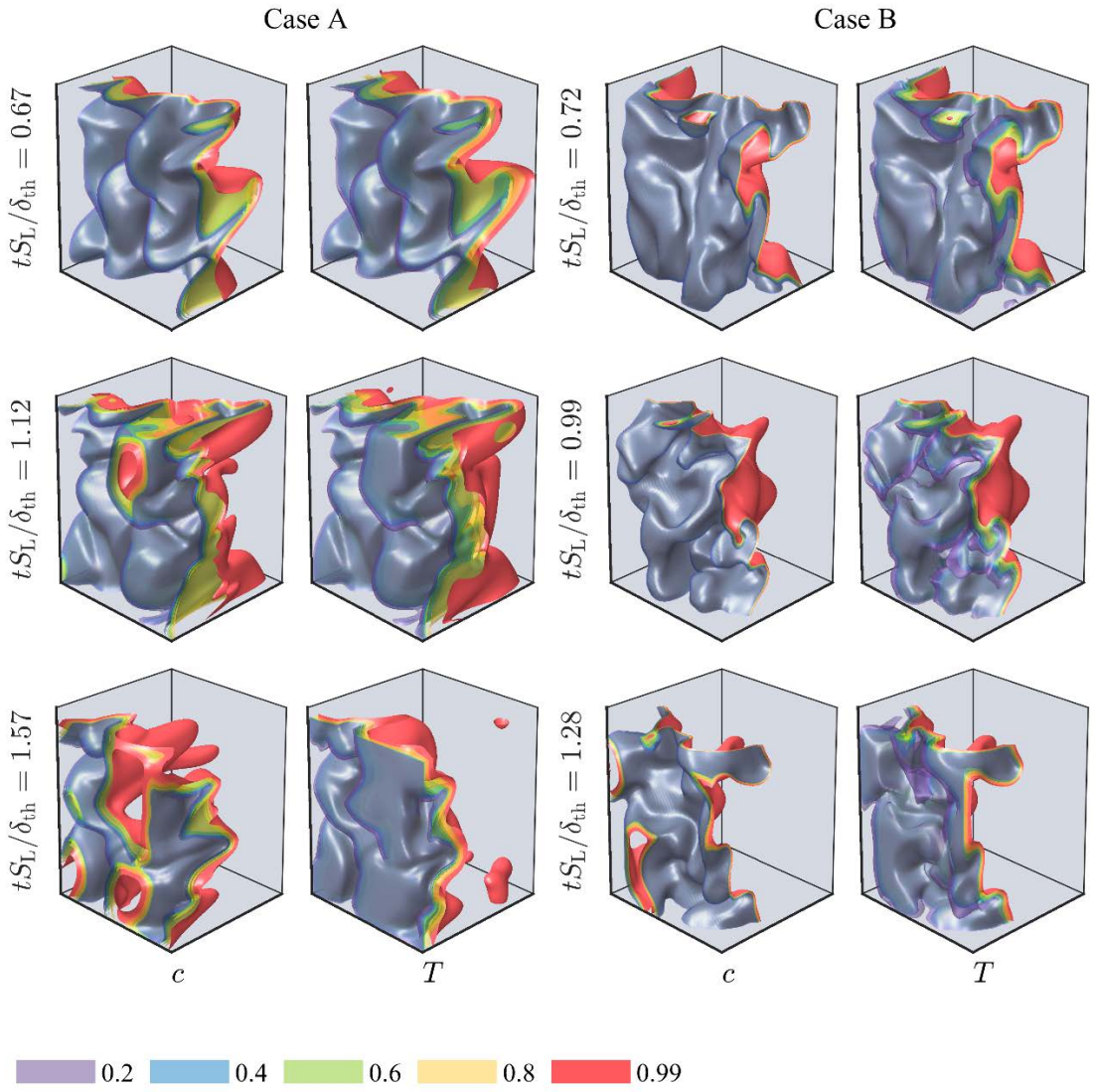

Figure 1. Distributions of c (based on fuel mass fraction) and non-dimensional temperature T at different time instants for (1st -2nd column) case A (stoichiometric hydrogen-air premixed flame), and (3rd -4th column) case B (stoichiometric methane-air premixed flame).

As the cases considered here are statistically planar flames with the mean direction of flame propagation aligning with x_1 −direction, the Reynolds/Favre averaging operation for a general quantity has been conducted in the homogeneous directions (i.e. over $x_2 - x_3$ planes) following several previous analyses (Zhang and Rutland, 1995; Veynante et al., 1997; Lai and Chakraborty, 2016a-b; Lai et al., 2017a-c, 2018).

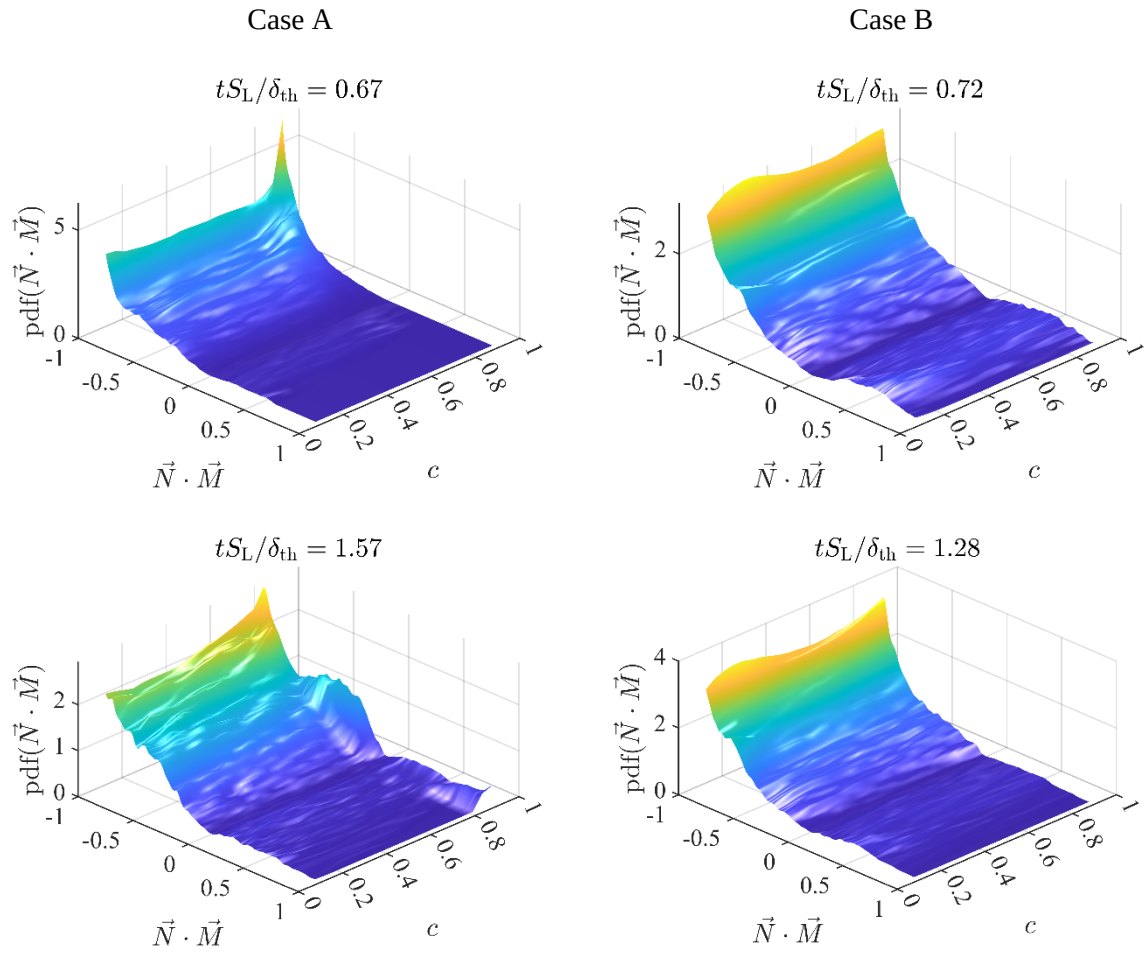

Figure 2. PDFs of $\vec{N} \cdot \vec{M}$ within the region given by $0.1 \leq c \leq 0.9$ for case A (1st column) at time $tS_L/\delta_{th} = 0.67$ (top) and 1.57 (bottom), case B (2nd column) at time $tS_L/\delta_{th} = 0.72$ (top) and 1.28 (bottom).

3. RESULTS & DISCUSSION

Flame-turbulence interaction

The isosurfaces of reaction progress variable c and non-dimensional temperature T at different time instants are exemplarily shown in Fig. 1 for cases A and B. The time instants, shown in Fig. 1 (and also in subsequent figures), are different for cases A and B because the flame propagates at different rates in these two cases and thus interacts with the wall at different time instants. The probability density functions (PDFs) of $\vec{N} \cdot \vec{M}$ for $0.1 \leq c \leq 0.9$ at two different time instants representing early and later stages of FWI are presented in Fig. 2 for cases A and B, where $\vec{N} = -\nabla c/|\nabla c|$ is the local flame normal vector and $\vec{M}$ is the wall normal vector. In this configuration, a value of $\vec{N} \cdot \vec{M} = -1.0$ is representative of head-on quenching of a perfectly planar flame propagating towards the wall. Moreover, the departure

of $\vec{N} \cdot \vec{M}$ from –1.0 also provides a measure of local flame wrinkling. It is evident from Fig. 2 that the PDFs of $\vec{N} \cdot \vec{M}$ peak at –1.0 for both cases for all time instants but the probability of finding $\vec{N} \cdot \vec{M} \neq -1.0$ increases with time, and this tendency is stronger in case A than in case B. At $t = 1.67\delta_{th}/S_L$, case A exhibits significant probabilities of finding $\vec{N} \cdot \vec{M} > 0.0$, indicating the roles of entrained flame elements in flame quenching, as suggested previously by Poinsot et al. (1993) and Zhao et al. (2018). However, this tendency is relatively weaker in case B due to smaller extent of flame wrinkling than in case A. Figure 2 indicates that there are local occurrences of sidewall and oblique-wall quenching in both cases although the flame-wall interaction in both cases takes place in predominantly head-on quenching mode. The likelihood of sidewall and oblique-wall quenching is higher in case A than in case B due to the greater extent of flame wrinkling in case A than in case B due to thermo-diffusive effects arising from $Le < 1$ species (e.g. H, H_2) in case A (see Lai et al., 2016a, Konstantinou et al., 2021 for $Le < 1$ effects in the context of simple chemistry).

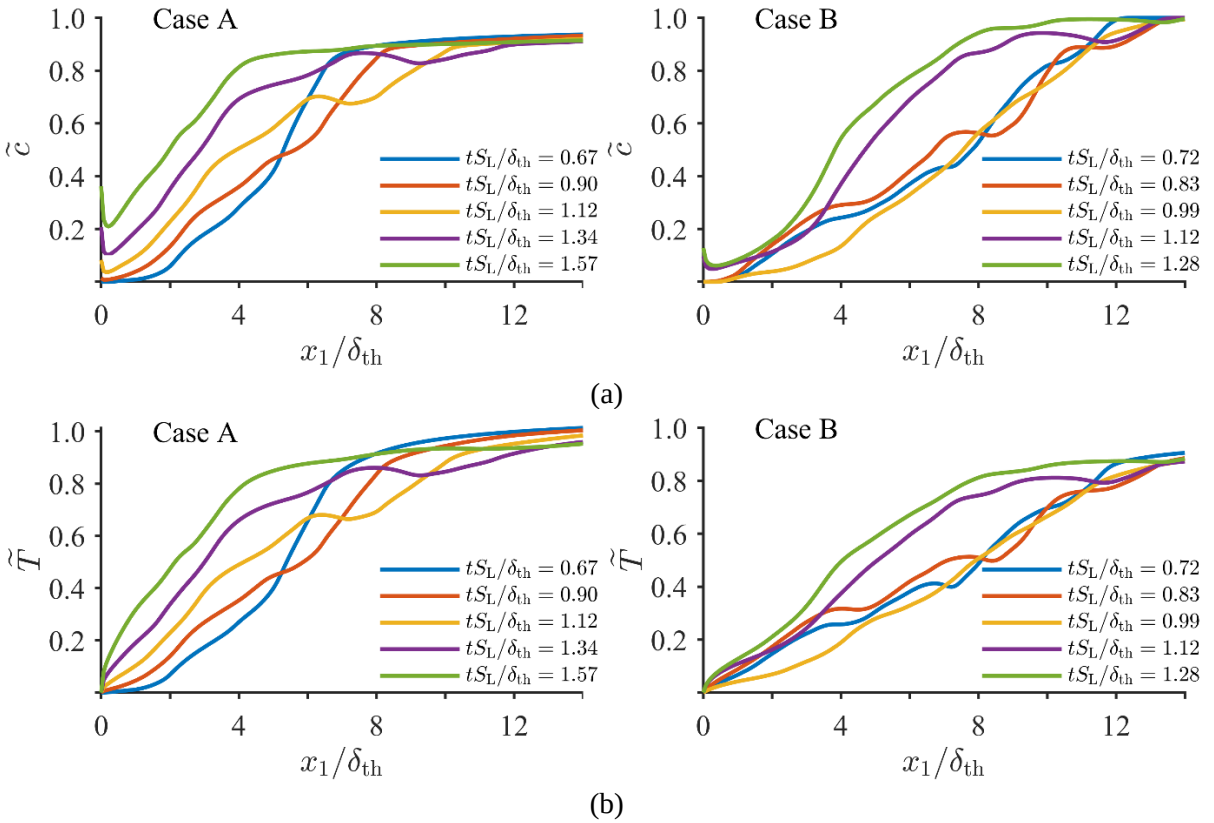

Figure 3. Variations of (a) $\tilde{c}$ and (b) $\tilde{T}$ with x_1/δ_{th} at different time instants for (left column) case A and (right column) case B.

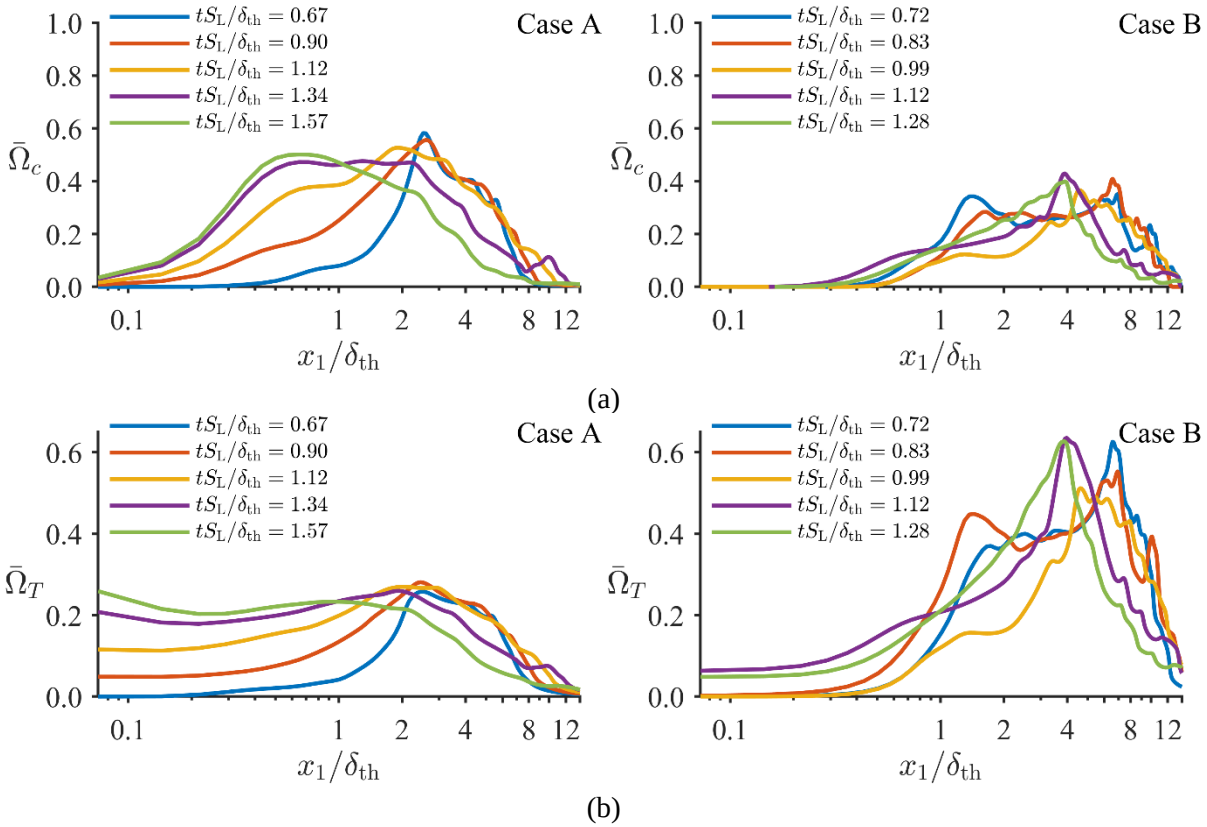

Figure 4. Variations of (a) $\overline{\Omega}_c = \overline{\dot{\omega}}_c \times \delta_{\mathrm{th}}/\rho_0 S_{\mathrm{L}}$ and (b) $\overline{\Omega}_T = \overline{\dot{\omega}}_T \times \delta_{\mathrm{th}}/\left[\rho_0 S_{\mathrm{L}} C_{p0} T_0\right]$ with normalised wall normal distance x_1/δ_{th} at different time instants for (left column) case A and (right column) case B.

It can further be seen from Fig. 1 that both c and T isosurfaces approach the wall as time progresses but the evolutions of c and T distributions take place at different rates. It can be appreciated from Fig. 1 that the distributions of c and T are qualitatively similar away from the wall but their distributions are significantly different in the vicinity of the wall for both cases A and B because the boundary conditions for temperature and fuel mass fraction are different at the wall. The wall normal component of the mass diffusion flux of the reaction progress variable vanishes at the wall, whereas a Dirichlet type boundary condition is imposed for temperature. These differences in boundary conditions for c and T lead to decoupling between these two quantities at the wall and a similar behaviour has been observed in previous simple chemistry DNS studies (Poinsot et al., 1993; Lai and Chakraborty, 2016a,b). The inequality between c and T is particularly stronger for the stoichiometric H_2-air premixed flame case (i.e. case A) than in the case of the stoichiometric $CH_4 -$ air premixed flame (i.e. case B) and the significant inequality between c and T can be observed in case A even when the flame is away from the wall due to differential diffusion of heat and species induced by light species such as H and H_2.

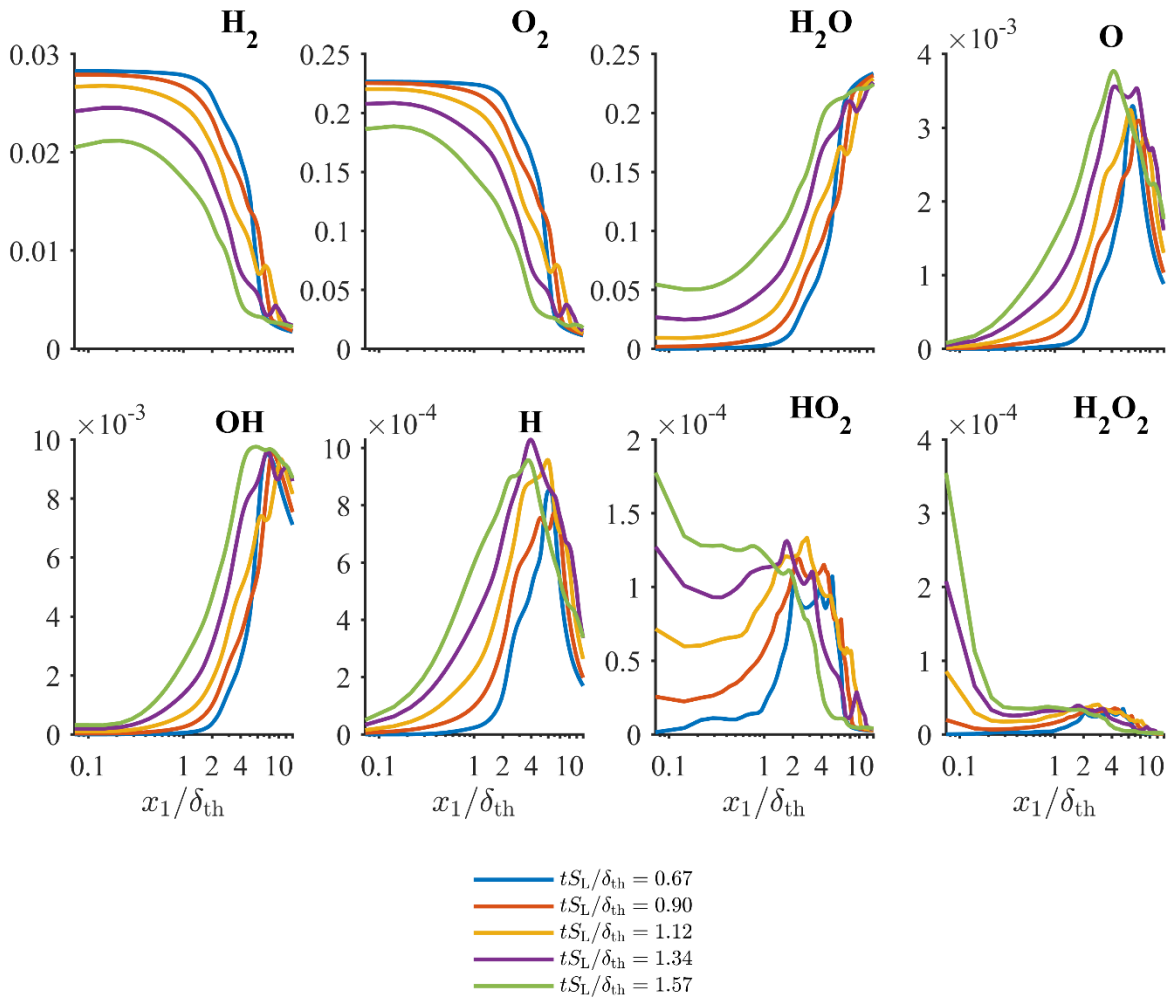

Figure 5. Variation of Favre-averaged mass fractions of $H_2, O_2, H_2O, O, OH, H, HO_2$ and H_2O_2 with the normalised wall normal distance x_1/δ_{th} at different time instants for head-on quenching of a turbulent stoichiometric hydrogen-air premixed flame (case A).

Distributions of Favre-averaged values of reaction progress variable and temperature

The decoupling between c and T is reflected also in their Favre-averaged counterparts $\tilde{c}$ and $\tilde{T}$, where $\tilde{q} = \overline{\rho q}/\bar{\rho}$ and $\bar{q}$ denote the Favre-averaged and Reynolds averaged values of a general quantity q, respectively. This can be substantiated from Figs. 3a and 3b where the variations of $\tilde{c}$ and $\tilde{T}$ with the normalised wall-normal distance x_1/δ_{th} are shown at different time instants, respectively. The corresponding variations of the mean normalised reaction rate of progress variable $\bar{\Omega}_c = \bar{\dot{\omega}}_c \times \delta_{\text{th}}/\rho_0 S_{\text{L}}$ and the normalised mean heat release rate $\bar{\Omega}_T = \bar{\dot{\omega}}_T \times \delta_{\text{th}}/(\rho_0 S_{\text{L}} C_{p0} T_0)$ (where $\dot{\omega}_T = -\sum_{i=1}^{N} \dot{\omega}_i h_{\text{f},i}^0$ is the dimensional heat release term with $\dot{\omega}_i, C_{p0}$ and $h_{\text{f},i}^0$ being the reaction rate, mixture specific heat at constant pressure in the unburned gas and enthalpy of formation of species i, respectively

and N is the total number of species) in the wall-normal direction are shown in Figs. 4a and 4b, respectively at different time instants for both cases A and B.

A comparison between $\tilde{c}$ and $\tilde{T}$ distributions in Fig. 3 reveals that $\tilde{T}$ vanishes at the wall (i.e. $x_1/\delta_{\mathrm{th}} = 0$), whereas the value of $\tilde{c}$ increases from $\tilde{c} = 0$ at the wall with time during the flame-wall interaction. This behaviour is a result of isothermal wall boundary condition and vanishing of the wall-normal diffusive flux of the reaction progress variable definition. This observation is consistent with previous findings for both laminar and turbulent flames (Lai and Chakraborty 2016a,b; Lai et al., 2018). A comparison between Figs. 3 and 4 reveals that $\overline{\Omega}_c$ either vanishes in case B or assumes negligible values in case A at the wall even when a non-zero value of $\tilde{c}$ is obtained at the wall. Thus, the increase in $\tilde{c}$ at the wall in case B does not arise due to chemical reaction but originates due to the diffusion of the unutilised fuel pockets from the quenching sites to the burned gas side. To explain higher $\tilde{c}$ values at the wall in case A than in case B, it is worthwhile to consider the variations of $\overline{\Omega}_c$ in the wall-normal direction. It can be seen from Fig. 4a that $\overline{\Omega}_c$ vanishes in the vicinity of the wall in the stoichiometric $CH_4 -$ air flame (i.e., in case B), whereas $\overline{\Omega}_c$ decreases as the wall is approached but a non-zero value is obtained at the wall during the flame-wall interaction in the stoichiometric H_2-air premixed flame case (i.e. case A). This non-zero value of $\overline{\Omega}_c$ leads to higher values of $\tilde{c}$ at the wall in case A than in case B where $\overline{\Omega}_c$ vanishes at the wall. It can further be seen by comparing Figs. 4a and 4b that $\overline{\Omega}_T$ does not vanish at the wall in both cases A and B even when $\overline{\Omega}_c$ assumes vanishingly small values in the near-wall region.

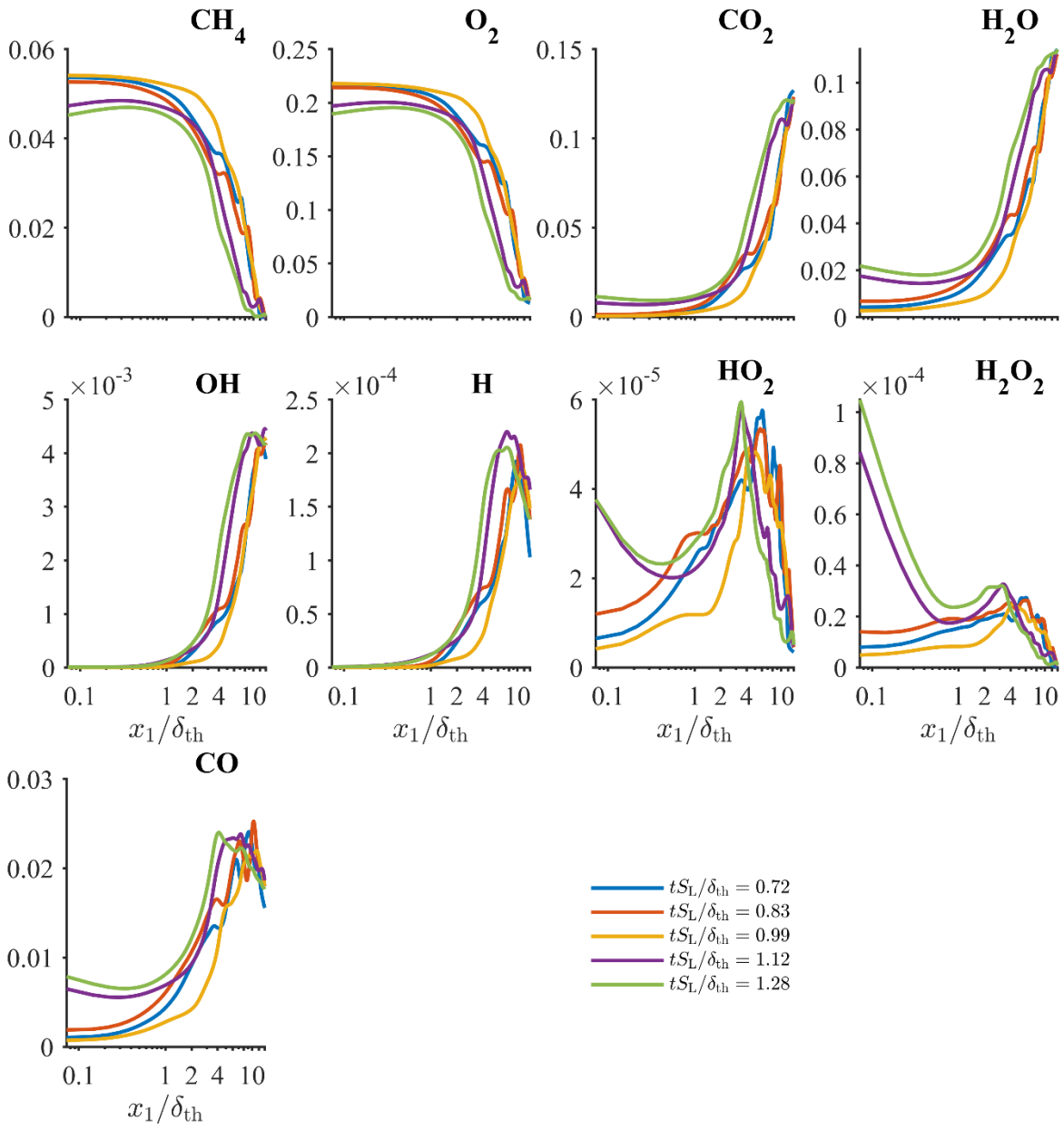

Figure 6. Variation of Favre-averaged mass fractions of $CH_4, O_2, CO_2, H_2O, OH, H, HO_2, H_2O_2$ and CO with the normalised wall normal distance x_1/δ_{th} at different time instants for head-on quenching of a turbulent stoichiometric methane-air premixed flame (case B).

A comparison between Figs. 3 and 4 indicates that $\overline{\Omega}_T$ remains vanishingly small at the wall at early times when the flame is away from the wall for both cases but $\overline{\Omega}_T$ assumes significant non-zero values at later times when the flame reaches the vicinity of the wall. This behaviour is particularly strong for the stoichiometric H_2-air premixed flame case (i.e., case A) where the magnitude of $\overline{\Omega}_T$ at the wall during flame-wall interaction becomes comparable to the peak values of $\overline{\Omega}_T$ when the flame is away

from the wall. By contrast, in the stoichiometric CH_4-air flame case (i.e., case B), the magnitude of $\overline{\Omega}_T$ at the wall during flame-wall interaction remains much smaller than the peak values of $\overline{\Omega}_T$ when the flame is away from the wall. However, a comparison between Figs. 3 and 4 reveals that high values of $\overline{\Omega}_T$ are obtained at high-temperature locations in case A when the flame is away from the wall, whereas at some stages of flame-wall interaction the peak value of $\overline{\Omega}_T$ can be found at the wall where the temperature is the lowest. Thus, the mechanism behind the high magnitudes of $\overline{\Omega}_T$ at the wall is expected to be significantly different to that when the flame is away from the wall, which leads to large values of $\overline{\Omega}_T$ within the flame.

Heat release rate at the wall

To explain the mechanism for heat release rate at the wall, the variations of major and important intermediate species mass fractions in the wall-normal direction at different time instants for cases A and B are shown in Figs. 5 and 6, respectively. It can be seen from Figs. 5 and 6 that both H_2 and CH_4 are depleted in the vicinity of the wall in cases A and B, respectively which is reflected in the increase of $\tilde{c}$ at the wall with time in Fig. 3.

The mass fractions of CO, OH and H remain small in the unburned gas, but they assume peak values within the flame before decreasing weakly towards the burned gas side in the case of the stoichiometric methane-air premixed flame case (i.e., case B) when the flame is away from the wall. The mass fractions of OH and H remain small at the wall when the flame is away from the wall, but these mass fractions increase in the wall-normal direction for both cases A and B. The OH radical is responsible for CO oxidation according to $CO+OH \rightarrow CO_2+H$ in case B, which also leads to the production of H, and this is crucial for chain branching reactions (e.g., $H+O_2 \rightarrow OH+O$; $O+H_2O \rightarrow OH+OH$) at high temperature. The absence of OH and low temperature in the near-wall region at the advanced stage of flame quenching give rise to the accumulation of CO in this region, where the CO oxidisation process becomes slower, and production of H from this chain stagnates. The near-wall accumulation of CO is consistent with previous experimental (Mann et al., 2014; Jainski et al., 2017a,b; Kosaka et al., 2020) and numerical (Palulli et al., 2019; Jiang et al., 2019,2021) studies.

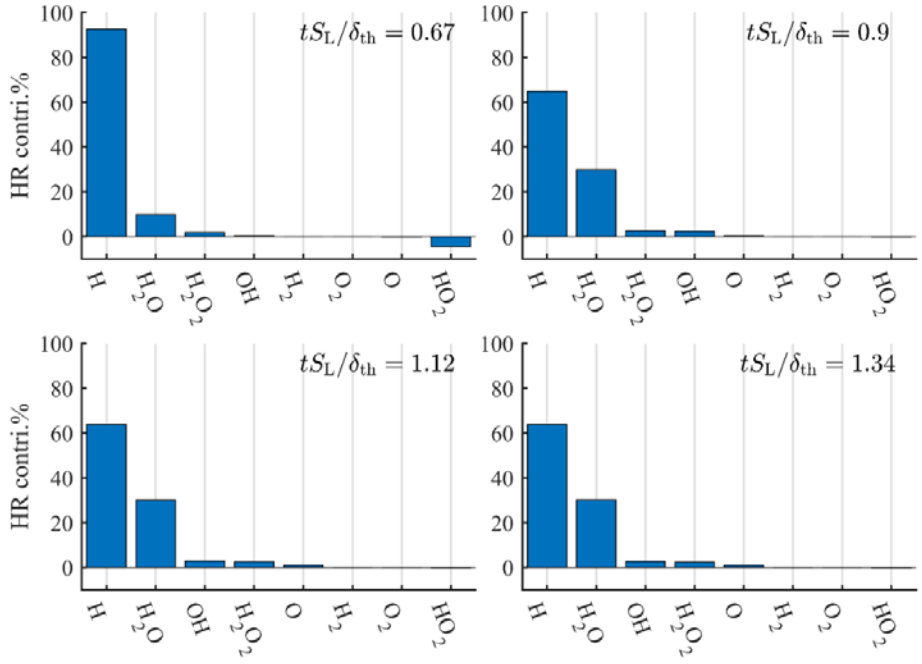

(a)

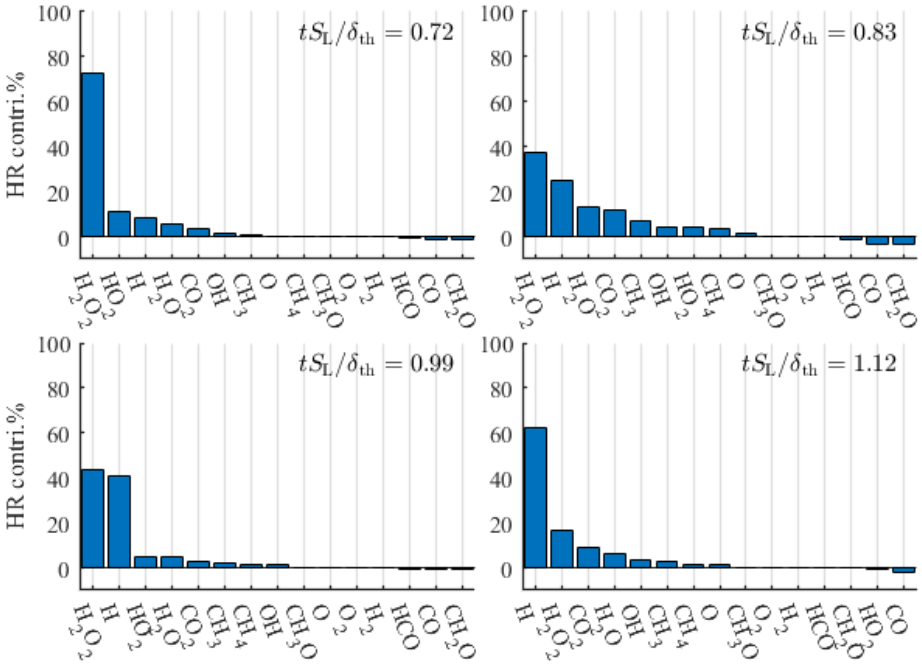

(b)

Figure 7. Percentage of the overall heat release at the wall arising from different species at different time instants for (a) case A and (b) case B.

Figures 5 and 6 show that the mass fractions of HO_2 and H_2O_2 exhibit significant increases at the wall during advanced stages of flame quenching for cases A and B. However, this tendency is particularly

prevalent in the stoichiometric H_2-air premixed flame-wall interaction. The reaction steps O_2+H+M→HO_2+M and 2HO_2→H_2O_2+O_2 can take place at a low temperature, and these reaction steps are responsible for the considerable rise of HO_2 and H_2O_2 concentrations at the wall. In the stoichiometric H_2-air premixed flame-wall interaction, the reactions H_2+OH→H_2O+H and H_2+O→OH+H can take place at relatively low temperatures if OH and O are supplied, and eventually, H is consumed in several intermediate chemical reactions (e.g. O_2+H+M→HO_2+M, H+O+M↔OH+M, H+OH+M↔H_2O+M), which can take place at low temperature during flame-wall interaction when O and OH diffuse to the near-wall region from the flame. This can be substantiated by the increases in H and H_2O concentration at the wall as the flame approaches the wall in the case of flame-wall interaction of the stoichiometric H_2-air premixed flame (i.e., case A). This consumption of H_2 at the wall in case A is reflected in the non-zero value of $\tilde{c}$ and non-zero value of $\overline{\Omega}_c$ at the wall.

The percentage shares of a given species α on the total mean heat release rate at the wall (i.e. $\%HR = -\overline{\dot{\omega}_\alpha} h_{f\alpha}^0 / \bar{\dot{\omega}}_T \times 100 = \overline{\dot{\omega}_\alpha} h_{f\alpha}^0 \times 100 / \sum_{\alpha=1}^{N} \overline{\dot{\omega}_\alpha} h_{f\alpha}^0$) at different time instants are shown in Figs. 7a and 7b for cases A and B, respectively. It can be seen from Fig. 7b that the heat release at the wall in the case of stoichiometric CH_4-air flame originates principally due to HO_2 and H_2O_2 due to low-temperature chemical reactions O_2+H+M→HO_2+M and 2HO_2→H_2O_2+O_2, which is consistent with previous findings (Lai et al., 2018). Figure 7a indicates that the heat release at the wall in case A arises principally due to H and H_2O, which is consistent with the increases of the concentration of these species at the wall with the progress of flame-wall interaction. Furthermore, the importance of O_2+H+M→HO_2+M, H+O+M↔OH+M, H+OH+M↔H_2O+M is reflected in the principal role played by H and H_2O on the near-wall heat release rate in case A. The chemical reactions H+O_2 ↔OH+O, H_2+O↔OH+H, H_2 + OH↔H_2O +H and H_2O + O↔OH+OH remain active for high temperatures, which includes chain branching reactions (e.g. H+O_2→OH+O; H_2O+O→OH+OH) and they are responsible for the heat release rate within the flame. At early times when the flame is away from the wall, H, OH and O are not available in the near-wall region (see Fig. 6) and thus the reactions O_2+H+M→HO_2+M, H+O+M↔OH+M, H+OH+M↔H_2O+M, H+HO_2↔2OH cannot take place at the wall. However, as time progresses and the flame comes in the vicinity of the wall, the chemical reactions such as

O_2+H+M→HO_2+M, H+O+M↔OH+M, H+OH+M↔H_2O+M, H+HO_2↔2OH can take place in the presence of O and OH, and accordingly lead to the heat release at the wall.

Wall heat flux and quenching distance

The near-wall behaviour of $\overline{\Omega}_c$ and $\overline{\Omega}_T$ influences the heat flux and the minimum wall-normal distance of the flame surface in the case of flame quenching. In this configuration, the flame-wall interaction can be characterised by the maximum value of the normalised wall heat flux magnitude Φ (i.e. $\Phi_{\max}$) and the minimum value of the Peclet number (i.e. $\mathrm{Pe}_{\min}$), which are defined as (Poinsot et al., 1993; Poinsot and Veynante, 2001; Lai and Chakraborty, 2016a,b; Lai et al., 2018):

$$\Phi = |q_{\mathrm{w}}|/\left[\rho_0 S_{\mathrm{L}} C_{p0}(T_{\mathrm{ad}} - T_0)\right] \quad \text{and} \quad \mathrm{Pe} = X/\delta_{\mathrm{th}} \tag{3}$$

where $q_{\mathrm{w}} = -\lambda\,(\partial\hat{T}/\partial x_1)_{\mathrm{w}}$ is the instantaneous wall heat flux with λ being the thermal conductivity, and X is the wall-normal distance of a predetermined T value (e.g. the non-dimensional temperature for which either the maximum value of reaction rate of c or the maximum heat release rate is obtained) for a 1D unstretched freely propagating premixed flame. The temporal evolutions of Φ and Pe during head-on quenching of both laminar and turbulent premixed flames have been presented elsewhere (Poinsot et al., 1993; Lai and Chakraborty., 2016a,b, Lai et al., 2018). The same qualitative behaviours have been observed here and thus are not explicitly shown for the sake of brevity but the maximum (minimum) values of Φ (Pe) will be discussed because of their importance in characterising the flame quenching process due to the wall heat loss.

The maximum values of Ω_c and Ω_T for a 1D unstretched stoichiometric $\mathrm{CH_4}$ −air premixed flame is obtained close to $T = 0.7$ (Liu et al., 2002), and thus the Peclet number for the stoichiometric $\mathrm{CH_4}$ −air premixed flame can be defined based on the wall-normal distance of the $T = 0.7$ isosurface. The minimum Peclet number for laminar head-on quenching of the stoichiometric $\mathrm{CH_4}$ −air premixed flame (i.e. $(\mathrm{Pe}_{\min})_{\mathrm{L}}$) is found to be 1.54, whereas the minimum value of the Peclet number $\mathrm{Pe}_{\min}$ for the turbulent simulation has been found to be 1.70. As the minimum Peclet number is indicative of the flame quenching distance, it can be inferred that the minimum quenching distance for the turbulent

head-on quenching of the stoichiometric CH_4 −air premixed flame considered here (i.e. case B) remains comparable to that obtained from the corresponding 1D laminar flame simulation, which is consistent with previous findings based on single-step chemistry with unity Lewis number (Lai et al., 2016a).

In contrast to the stoichiometric CH_4 −air premixed flame, the maximum value of Ω_c is obtained at $T \approx 0.5$, whereas the maximum value of Ω_T is attained at $T \approx 0.3$ for a 1D unstretched stoichiometric H_2 −air premixed flame. The minimum Peclet number for 1D laminar head-on quenching of the stoichiometric H_2 −air premixed flame based on the wall-normal distance of the $T = 0.3$ ($T = 0.5$) isosurface is 0.13 (0.38). However, the minimum Peclet number Pe_{min} based on the $T = 0.3$ ($T = 0.5$) isosurface during head-on quenching of turbulent stoichiometric H_2 −air flame is found to be 0.11 (0.24). This suggests that the minimum quenching distance decreases under turbulent conditions in the stoichiometric H_2 −air premixed flame, which is consistent with the decrease in the minimum quenching distance under turbulent conditions for $Le < 1$ simple chemistry DNS (Lai and Chakraborty, 2016a). The flame elements, which are convexly curved towards the reactants, remain close to the wall because of the geometric configuration of head-on-quenching. The differential diffusion effects induced by faster diffusion of reactants than the thermal diffusion rate in the regions, which are convexly curved towards the reactants, give rise to relatively higher rates of heat release and higher temperature in these regions in the stoichiometric H_2 − air premixed flame than in the corresponding laminar flame (e.g. $T \approx 0.5$ is associated with $c = 0.75$ in the stoichiometric H_2 −air premixed flame), which is similar to the flames with characteristic Lewis number smaller than unity (i.e. Le <1) (Rutland and Trouve, 1993; Chakraborty and Cant, 2005; Lai and Chakraborty, 2016a; Konstantinou et al., 2021). This can be substantiated from Fig. 8 where the instantaneous $c = 0.75$ isosurfaces coloured by non-dimensional temperature T are shown for cases A and B at different time instants. Therefore, the turbulent flame elements, which are convexly curved towards the reactants, can potentially resist the heat loss through the wall and can reach closer to the wall before quenching than in the case of head-on-quenching of the corresponding planar laminar flame.

It can further be seen from Fig. 8 that there is a variation of non-dimensional temperature also on the $c = 0.75$ isosurface even for the stoichiometric CH_4 −air premixed flame, where the relatively high temperature zones are associated with the regions which are concave to the fresh reactants. By contrast, relatively low temperature values are obtained at the zones which are convex to the fresh reactants in case B (see Fig. 8). This behaviour is analogous to $Le > 1$ flames in the context of simple chemistry simulations where the faster focusing of heat fluxes than the defocusing of mass fluxes of the reactants at the regions which are concavely curved regions leads to high values of reaction rate magnitudes and temperatures (Rutland and Trouve, 1993; Chakraborty and Cant, 2005; Lai and Chakraborty, 2016a; Konstantinou et al., 2021). The presence of $Le > 1$ species such as CO and CO_2 along with heavier hydrocarbons (e.g. C_2H_2, C_2H_4 and C_2H_6) in the reaction zone for the stoichiometric $CH_4 -$ air premixed flame induces the behaviour analogous to $Le > 1$ flames. As the low temperature zones face the wall in the stoichiometric CH_4 −air premixed flame in contrast to high temperature zones in the stoichiometric H_2 −air premixed flame, the flame in case B quenches more readily than in case A. This also explains the larger flame quenching distance in the stoichiometric $CH_4 -$ air premixed flame than in the stoichiometric $H_2 -$ air premixed flame.

It is worth noting that the spatial distribution of temperature in the laminar premixed stoichiometric $CH_4 -$ air premixed flame is significantly different from that in the laminar premixed stoichiometric $H_2 -$ air premixed flame. In the $CH_4 -$ air premixed flame, a high-temperature gradient is obtained close to the burned gas side of the flame where the maximum heat release rate is obtained (e.g. $T \approx 0.7$), whereas the temperature gradient remains small for $T > 0.3$ in the stoichiometric H_2 −air premixed flame (Liu et al., 2002). Thus, the minimum Peclet number based on the T isosurface corresponding to the maximum heat release in the stoichiometric $H_2 -$ air premixed flame turns out to be smaller than that in the case of a $CH_4 -$ air premixed flame for both laminar and turbulent conditions. This is consistent with previous findings by Dabireau et al. (2003) and Gruber et al. (2010).

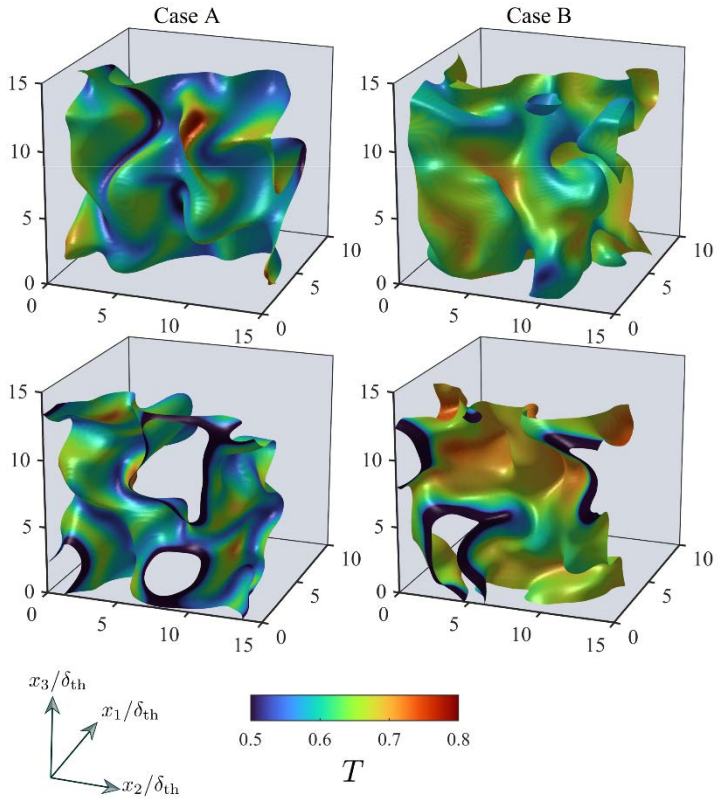

Figure 8. Instantaneous views of the $c = 0.75$ isosurface coloured by the local non-dimensional temperature T for case A (1st column) at time $tS_{\rm L}/\delta_{\rm th} = 0.67$ (top) and 1.57 (bottom), case B (2nd column) at time $tS_{\rm L}/\delta_{\rm th} = 0.72$ (top) and 1.28 (bottom),

In head-on-quenching, the instant when the minimum Peclet number is obtained coincides almost with the attainment of the maximum value of the normalised wall heat flux magnitude $\Phi_{\rm max}$. The maximum value of the normalised wall heat flux magnitude $\Phi_{\rm max}$ for 1D laminar head-on quenching for the stoichiometric $CH_4 -$ air premixed flame has been found to be 0.47, whereas a comparable value (i.e., $\Phi_{\rm max} = 0.48$) is obtained during the flame-wall interaction of the corresponding turbulent flame. In the turbulent head-on-quenching case, there are more flame surface elements in the vicinity of the wall due to flame wrinkling and thus the maximum heat flux value can be greater than the corresponding value for the 1D head-on-quenching simulation. However, for both laminar and turbulent head-on-quenching of the stoichiometric CH_4 −air premixed flames, $\Phi_{\rm max}$ roughly scales with $1/{\rm Pe}_{\rm min}$ (i.e. $\Phi_{\rm max} \sim 1/{\rm Pe}_{\rm min}$), which is consistent with previous findings based on single-step chemistry (Poinsot et al., 1993; Lai and Chakraborty, 2016a,b; Lai et al., 2018). By contrast, $\Phi_{\rm max}$ for head-on quenching of the turbulent stoichiometric H_2 −air premixed flame case (i.e., case A) is found to be 0.15, whereas the value in the corresponding case of laminar 1D head-on quenching is 0.12. These $\Phi_{\rm max}$ values in the

case of head-on quenching of stoichiometric H_2 −air premixed flames are smaller than $1/\mathrm{Pe}_{\mathrm{min}}$. This behaviour can be explained in the following manner. The maximum heat flux magnitude scales as: $|q_{\mathrm{w}}| \sim \lambda \Delta T/X$, where ΔT is the dimensional temperature rise over the quenching distance X. This suggests that Φ_{max} can be taken to scale as:

$$\Phi_{\mathrm{max}} \sim \delta_{\mathrm{z}} \Delta T/[(T_{\mathrm{ad}} - T_0)X] \sim (\delta_{\mathrm{z}}/\delta_{\mathrm{th}}) Pe_{\mathrm{min}}^{-1} \Delta T/(T_{\mathrm{ad}} - T_0) \quad (4)$$

where $\delta_{\mathrm{Z}} = \alpha_{T0}/S_{\mathrm{L}}$ is the Zel'dovich flame thickness with α_{T0} being the unburned gas thermal diffusivity. In the stoichiometric CH_4 − air premixed flame $\Delta T/(T_{\mathrm{ad}} - T_0)$ remains of the order of unity (≈0.7), whereas this ratio is much smaller than unity (≈0.3) for the stoichiometric H_2 − air premixed flame. Moreover, $(\delta_{\mathrm{th}}/\delta_{\mathrm{z}})$ in the stoichiometric H_2 −air premixed flame is much greater than in the stoichiometric CH_4 − air premixed flame, which also contributes to smaller values of Φ_{max} in the stoichiometric H_2 − air premixed flame in comparison to that in the stoichiometric CH_4 −air premixed flame. This is also consistent with previous findings by Dabireau et al. (2003) and Gruber et al. (2010). Thus, the scaling $\Phi_{\mathrm{max}} \sim 1/\mathrm{Pe}_{\mathrm{min}}$ cannot be used for the stoichiometric H_2 −air premixed flame.

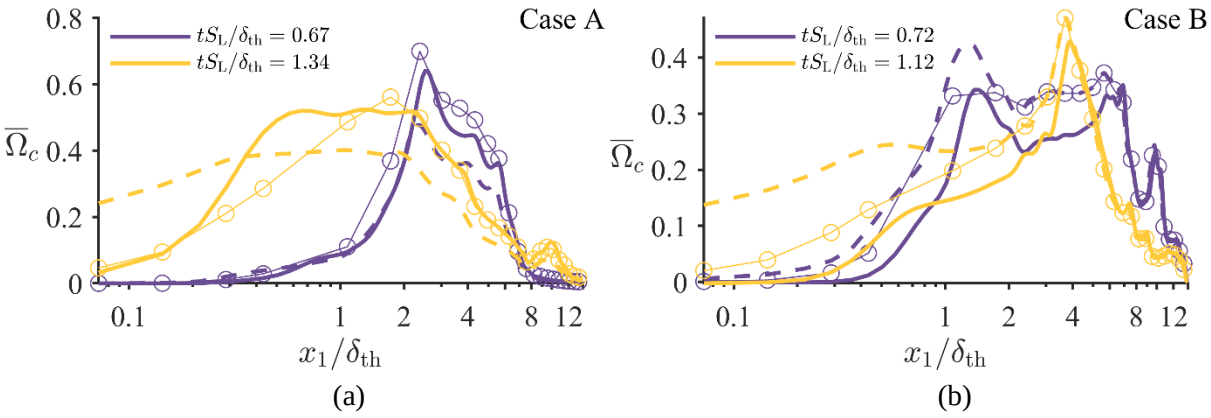

Figure 9. Variations of $\overline{\Omega}_c$ (——), $\rho_0 S_L \Sigma_{\mathrm{gen}} \times \delta_{th}/\rho_0 S_L$ (— —), and the prediction of Eq. 6 (—○ —), with normalised wall normal distance x_1/δ_{th} at different time instants for (a) case A and (b) case B.

FSD based mean reaction rate closure in the near-wall region

The differences in thermo-chemistry and heat transfer characteristics between the head-on-quenching of stoichiometric CH_4 − air and stoichiometric H_2 − air premixed flames revealed by the foregoing discussion are likely to have implications on the near-wall modelling of mean reaction rate. The mean

reaction rate $\bar{\dot{\omega}}$ in turbulent premixed flames away from the wall is often modelled with the help of generalised FSD $\Sigma_{\mathrm{gen}} = \overline{|\nabla c|}$ (Boger et al., 1998) as:

$$\bar{\dot{\omega}}_c \approx \overline{(\rho S_{\mathrm{d}})}_{\mathrm{s}} \Sigma_{\mathrm{gen}} \tag{5}$$

where $\overline{(Q)}_{\mathrm{s}} = \overline{Q|\nabla c|}/\Sigma_{\mathrm{gen}}$ indicates a surface-averaging operation and $S_{\mathrm{d}} = (\mathrm{D}c/\mathrm{D}t)/|\nabla c|$ is the displacement speed (Boger et al., 1998). The quantity $\overline{(\rho S_{\mathrm{d}})}_s$ is often modelled as $\overline{(\rho S_{\mathrm{d}})}_{\mathrm{s}} \approx \rho_0 S_{\mathrm{L}}$ (Boger et al., 1998; Hawkes and Cant, 2001). The temporal evolutions of $\left(\rho_0 S_{\mathrm{L}}\, \Sigma_{\mathrm{gen}}\right) \times \delta_{\mathrm{th}}/\rho_0 S_L$ in the wall-normal direction are compared to $\bar{\Omega}_c$ in Fig. 9, which shows that $\rho_0 S_{\mathrm{L}} \Sigma_{\mathrm{gen}}$ overpredicts $\bar{\dot{\omega}}_c$ in the near-wall region and predicts the non-zero value of the mean reaction rate at the wall for both cases A and B. This behaviour is also consistent with previous findings based on simple chemistry (Alshaalan et al., 1998; Bruneaux et al., 1996,1997; Sellmann et al., 2017). It can be noted that in the derivation of Eq. 5 it is assumed that the mean molecular diffusion rate $\overline{\nabla \cdot (\rho D \nabla c)}$ remains negligible in comparison to the mean reaction rate $\bar{\dot{\omega}}_c$ (i.e. $\bar{\dot{\omega}}_c \gg \overline{\nabla \cdot (\rho D \nabla c)}$) but this is not necessarily the case in the near-wall region in the case of head-on quenching because $\bar{\dot{\omega}}_c$ vanishes but $\overline{\nabla \cdot (\rho D \nabla c)}$ does not in the flame quenching zone.

Sellmann et al. (2017) demonstrated that the models proposed by Alshaalan *et al.* (1998) and Bruneaux et al. (1996,1997) do not adequately capture the near-wall behaviour of $\bar{\Omega}_c$ in head-on quenching and the same behaviour has been observed here and thus is not shown here for the sake of brevity. Sellmann et al. (2017) proposed a new model expression for the FSD based $\bar{\dot{\omega}}_c$ closure based on simple chemistry, which was found to predict the mean reaction rate for a range of different conditions in terms of turbulence intensity and global Lewis number. The model expression by Sellmann et al. (2017) is given as:

$$\bar{\dot{\omega}}_c = A_1 Le^{-1} \rho_0 S_{\mathrm{L}} \Sigma_{\mathrm{gen}}, \text{ where } A_1 = 0.5[\mathrm{erf}\,(x_1/\delta_Z - 0.7\Pi) + 1] \tag{6}$$

$$\text{and } \Pi = (Pe_{\mathrm{min}})_{\mathrm{L}} \delta_{\mathrm{th}}/\delta_z [\mathrm{erf}(8Le - 6.0) + 1]/2$$

Here, Le refers to the Lewis number of the species based on which c is defined, $(Pe_{\mathrm{min}})_{\mathrm{L}}$ is the Peclet number evaluated based on the wall-normal distance of $T = 0.3$ ($T = 0.7$) isosurface for case A (case

B) according to the previous discussion on the minimum Peclet number. Figure 9 shows that Eq. 6 satisfactorily predicts the variation of $\bar{\dot{\omega}}_c$ both away from and close to the wall for both cases A and B. Thus, the FSD based reaction rate closure proposed previously based on *a-priori* analysis of simple chemistry DNS data is found to be valid also for detailed chemistry simulations of head-on quenching, which is consistent with previous computational findings (Lai et al., 2018).

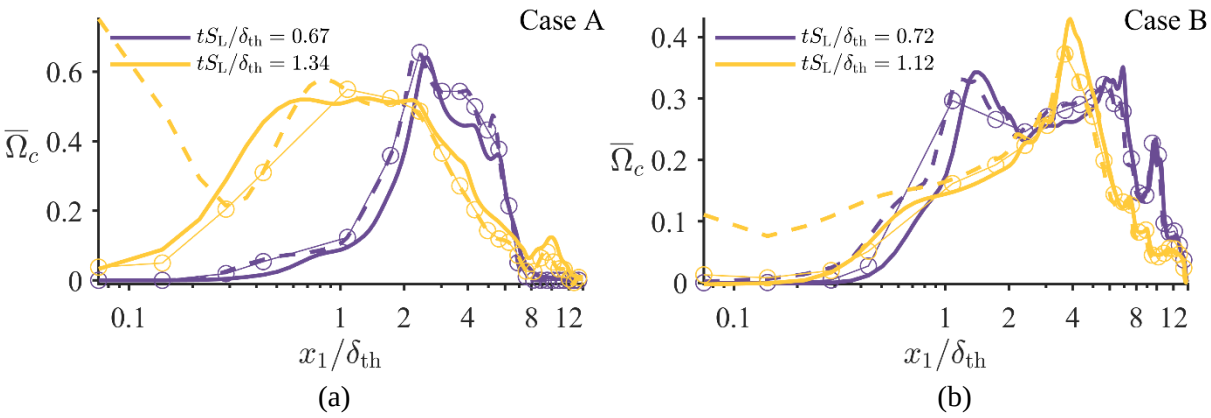

Figure 10. Variations of $\overline{\Omega}_c$ (——), $2\bar{\rho}\tilde{\varepsilon}_c/(2c_m - 1) \times \delta_{th}/\rho_0 S_L$ (— —), and the prediction of Eq. 8 (—○ —), with normalised wall normal distance x_1/δ_{th} at different time instants for (a) case A and (b) case B.

Scalar dissipation rate (SDR) based mean reaction rate closure in the near-wall region

Another alternative mean reaction rate closure was proposed by Bray (1980) using the scalar dissipation rate in the following manner:

$$\bar{\dot{\omega}}_{\mathrm{c}} = 2\bar{\rho}\tilde{\varepsilon}_c/(2c_{\mathrm{m}} - 1) \tag{7}$$

where $\tilde{\varepsilon}_c = \overline{\rho D \nabla c'' \cdot \nabla c''}/\bar{\rho}$ is the unresolved SDR, and $c_{\mathrm{m}} = \int_0^1 [\dot{\omega}c]_{\mathrm{L}} f(c)\mathrm{d}c \,/\, \int_0^1 [\dot{\omega}]_{\mathrm{L}} f(c)\mathrm{d}c$ is a thermo-physical parameter (0.75 and 0.87 in cases A and B, respectively) with $f(c)$ being the burning-mode PDF. Equation 7 was originally derived for $Da \gg 1$ where a presumed bimodal distribution with impulses at $c = 0.0$ and $c = 1.0$ can be taken to approximate the PDF of c. However, Chakraborty and Cant (2011) demonstrated based on scaling arguments that Eq. 7 remains valid also for $Da < 1$ combustion within the flamelet regime. The variations of $2\bar{\rho}\tilde{\varepsilon}_c/(2c_{\mathrm{m}} - 1) \times \delta_{\mathrm{th}}/\rho_0 S_{\mathrm{L}}$ with the normalised wall-normal distance x_1/δ_{th} at different time instants are compared to the corresponding $\overline{\Omega}_c$ variations in Fig. 10, which shows that Eq. 7 predicts $\bar{\dot{\omega}}_{\mathrm{c}}$ satisfactorily when the flame is away from

the wall (e.g. $tS_L/\delta_{th} = 0.67$ and 0.72 in cases A and B, respectively). However, Eq. 7 does not capture $\overline{\Omega}_c$ variations and overpredicts the mean reaction rate significantly in the near-wall region showing non-zero values at the wall when the flame starts to interact with the wall (e.g. $tS_L/\delta_{th} = 1.34$ and 1.12 in cases A and B, respectively).

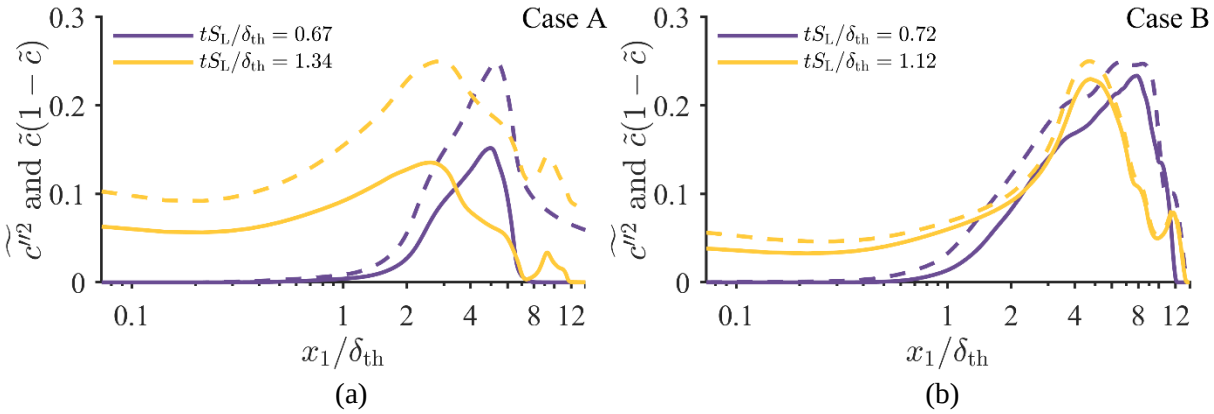

Figure 11. Variations of $\widetilde{c''^2}$ (——), $\tilde{c}(1-\tilde{c})$(— —) with normalised wall normal distance x_1/δ_{th} at different time instants for (a) case A and (b) case B.

The deviation of $\widetilde{c''^2}$ from $\tilde{c}(1-\tilde{c})$ provides the measure of the departure of the pdf of c from a bi-modal distribution with impulses at $c = 0.0$ and $c = 1.0$, and also from the high Damköhler number limit. Figure 11 shows the variations of $\widetilde{c''^2}$ and $\tilde{c}(1-\tilde{c})$ with the normalised wall-normal distance x_1/δ_{th} at different time instants, which shows that $\widetilde{c''^2}$ is smaller than $\tilde{c}(1-\tilde{c})$ even when the flame is away from the wall due to Da < 1 combustion and this behaviour is sustained in the near-wall region during flame-wall interaction. Thus, the PDF of c does not follow a bimodal distribution, and the flamelet assumption is rendered invalid during flame quenching, which indicates that Eq. 7 cannot be used in the near-wall region during flame quenching (Gruber et al., 2010; Lai and Chakraborty, 2016a,b). Lai and Chakraborty (2016a,b) modified Eq. 7 for the near-wall region based on simple chemistry DNS data as:

$$\overline{\dot{\omega}} = \frac{2\bar{\rho}\widetilde{\varepsilon_c}}{2c_m - 1} A_2 \exp\left(\tilde{c} - \tilde{T}\right) + B_2 C_2 \rho_0 S_L \sqrt{\frac{\widetilde{\varepsilon_c}}{\widetilde{D}}} \exp\left[-0.5\left(\frac{x_1}{\delta_Z} - \Pi\right)^2\right] \quad (8i)$$

The model parameters A_2, B_2 and C_2 are given by:

$A_2 = 0.5\{\text{erf}[3.0(x_1/\delta_\text{Z} - \Pi)] + 1\}$, $B_2 = 0.5[\text{erf}(x_1/\delta_Z - \Pi) + 1]$ and $C_2 = 2.31\text{erf}\left[2.6\left(\tilde{c} - \tilde{T}\right)\right]$ (8ii)

It is worth noting that $(\tilde{c} - \tilde{T})$ remains relatively small for $x_1/\delta_\text{th} \gg \left(Pe_{\text{min,}}\right)_L$, which leads to $A_2 \exp\left(\tilde{c} - \tilde{T}\right) \approx 1.0$ and $B_2 C_2 = 0$, reducing Eq. 8i to Eq. 7 away from the wall. The second term on the right-hand side of Eq. 8i becomes significant when $(\tilde{c} - \tilde{T})$ assumes large values in the vicinity of the wall during flame quenching (Lai and Chakraborty, 2016a,b; Lai et al., 2018). It can be seen from Fig. 10 that Eq. 8 satisfactorily predicts $\overline{\Omega}_c$ for both cases A and B when $\widetilde{\varepsilon_c}$ is directly computed from DNS data. However, $\widetilde{\varepsilon_c}$ also needs closure and recently Lai and Chakraborty (2016a,b) modified an existing model for $\widetilde{\varepsilon_c}$ (Kolla et al., 2009; Chakraborty and Swaminathan, 2011) for head-on quenching using *a-priori* analysis of simple chemistry DNS data:

$$\widetilde{\varepsilon_c} = \frac{A_\epsilon \exp\left[-1.2Le\left(\tilde{c}_\text{w} - \tilde{T}_\text{w}\right)^3\right]}{\beta'}\left(2K_c^* \text{Le}^{-1.88}\frac{S_\text{L}}{\delta_\text{th}} + C_3\frac{\tilde{\varepsilon}}{\tilde{k}} - \tau\frac{C_4(1-\tilde{c})^\Phi}{Le^{2.57}}\frac{S_\text{L}}{\delta_\text{th}}\right)\tilde{c}\,(1-\tilde{c}) \quad \text{(9i)}$$

Here, $\tilde{q}_\text{w}$ refers to the Favre mean value at the wall for a quantity q at a given instant of time and K_c^* is a thermo-chemical parameter which is given by (Kolla et al., 2009):

$$K_c^* = \frac{\delta_\text{th}}{S_\text{L}}\frac{\int_0^1[\rho(D\nabla c\cdot\nabla c)\nabla\cdot\vec{u}f(c)]_\text{L}\text{d}c}{\int_0^1[\rho(D\nabla c\cdot\nabla c)f(c)]_\text{L}\text{d}c} \quad \text{(9ii)}$$

The parameter K_c^* is equal to 0.60τ and 0.87τ in cases A and B, respectively), $A_\epsilon = 0.5[\text{erf}(x_1/\delta_\text{Z} - \Pi) + 1]$ is a model parameter in Eq. 9i such that $A_\epsilon \exp\left[-1.2\text{Le}\left(\tilde{c}_\text{w} - \tilde{T}_\text{w}\right)^3\right] \neq 1$ in the near-wall region and reduces to 1.0 away from the wall. Kolla et al. (2009) and Chakraborty and Swaminathan (2011) suggested:

$$\Phi = 0.2 + 1.5(1 - Le),\ \beta' = 6.7,\ C_3 = 1.5\sqrt{\text{Ka}_\text{L}}/\left(1 + \sqrt{\text{Ka}_\text{L}}\right) \text{ and } C_4 = 1.1/(1 + \text{Ka}_\text{L})^{0.4} \quad \text{(10)}$$

where $\text{Ka}_\text{L} = (\delta_\text{th}\tilde{\varepsilon}/S_\text{L}^3)^{1/2}$ is the local Karlovitz number and $\tilde{\varepsilon}$ is the dissipation rate of turbulent kinetic energy $\tilde{k}$. Further information on the derivation of Eqs. 8-9 can be found elsewhere (Kolla et al., 2009; Lai and Chakraborty, 2016a,b) and thus is not repeated here.

The predictions of Eq. 9 are compared to $\widetilde{\varepsilon_c} \times \delta_{\mathrm{th}}/S_{\mathrm{L}}$ extracted from DNS data for cases A and B in Fig. 12 for different time instants, which shows a satisfactory agreement with DNS data both near and away from the wall for the stoichiometric CH_4 −air premixed flame case (i.e. case B) but this model does not perform well especially in the near-wall region during the flame-wall interaction in the stoichiometric H_2 −air premixed flame case (i.e. case A). Moreover, some quantitative disagreement between Eq. 9 and $\widetilde{\varepsilon_c}$ extracted from DNS data can be seen in case A even when the flame is away from the wall. Therefore, the applicability of the algebraic closure $\widetilde{\varepsilon_c}$ remains questionable for flames where the non-unity Lewis number effects are strong due to the availability of light species (e.g., H_2 − air premixed flames). Sellmann et al. (2017) and Lai et al. (2016c) proposed transport equation based FSD and SDR closures, respectively for non-unity Lewis number flames using simple chemistry DNS data. The assessment of these closures in the context of detailed chemistry DNS data is beyond the scope of the current analysis but will form the foundation of further analysis. Furthermore, it can be appreciated from Fig. 4 that the profiles of $\overline{\Omega}_c$ and $\overline{\Omega}_T$ are both qualitatively and quantitatively similar in the stoichiometric CH_4 − air premixed flame case (i.e., case B) but that is not the case for the stoichiometric H_2 − air premixed flame (i.e., case A). Thus, it may not be sufficient to model $\overline{\dot{\omega}}_c$ for the closure of $\overline{\dot{\omega}}_T$ for the stoichiometric H_2 − air flame case because $\overline{\dot{\omega}}_c$ closure deals with major species but that is not sufficient to capture the important role played by intermediate species in the head-on quenching of stoichiometric H_2 − air premixed flames. Thus, further analyses will be needed for the closure of $\overline{\dot{\omega}}_T$ for the premixed flame-wall interaction of H_2 − air flames.

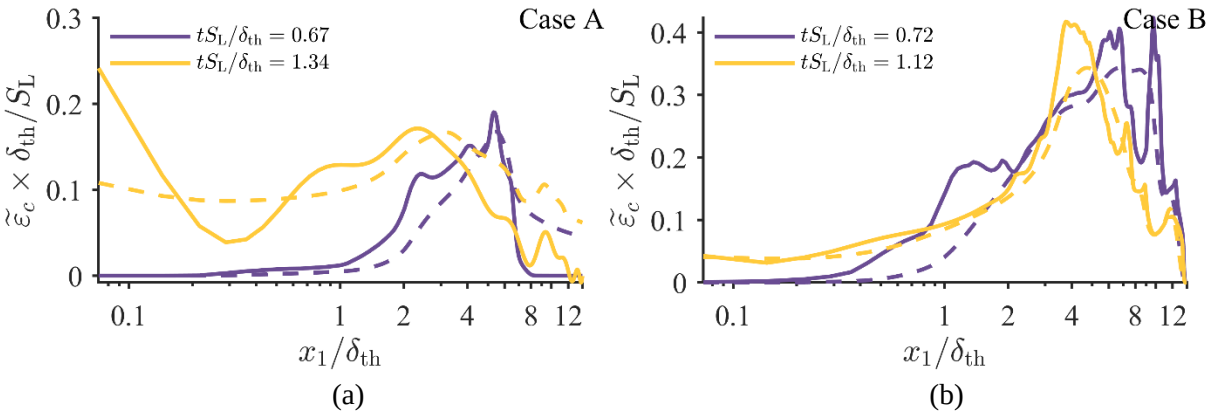

Figure 12. Variations of $\widetilde{\varepsilon_c} \times \delta_{\mathrm{th}}/S_{\mathrm{L}}$ (——) and the prediction of Eq. 9 (— —) with normalised wall normal distance x_1/δ_{th} at different time instants for (a) case A and (b) case B.

4. CONCLUSIONS

The statistical behaviour of the head-on quenching of a stoichiometric H_2 −air premixed flame by an inert isothermal wall is compared to that in the case of a stoichiometric CH_4 −air premixed flame under both laminar and turbulent conditions with the same turbulence intensity and length scale ratio away from the wall. The main findings are as follows:

- A significant amount of inequality between the reaction progress variable and the non-dimensional temperature has been found to prevail in the near-wall region for both stoichiometric methane-air and hydrogen-air premixed flames. However, the extent of this inequality is relatively greater in the stoichiometric hydrogen-air flame than in the stoichiometric methane-air flame and this inequality is obtained also away from the wall for the stoichiometric hydrogen-air premixed flame.
- It has been found that the mean heat release rate does not vanish at the wall in head-on quenching of both stoichiometric methane-air and hydrogen-air premixed flames even when the mean reaction rate of reaction progress variable defined based on fuel mass fraction assumes vanishingly small values in the near-wall region. This behaviour is particularly strong for the stoichiometric hydrogen-air flame case where the mean heat release rate at the wall could become comparable to the corresponding value within the reaction zone when the flame is away from the wall.
- The heat release at the wall in the case of the stoichiometric CH_4 −air premixed flame arises principally due to HO_2 and H_2O_2 caused by low-temperature chemical reactions $O_2+H+M\rightarrow HO_2+M$ and $2HO_2\rightarrow H_2O_2+O_2$ and the lack of OH in the vicinity of the wall gives rise to a high concentration of CO in the near-wall region, because of the absence of $CO+OH\rightarrow CO_2+H$. It has been found that HO_2 and H_2O_2 exhibit significant increases in concentration at the wall during advanced stages of flame quenching for both stoichiometric methane-air and hydrogen-air premixed flames, and this tendency is particularly prevalent in the stoichiometric H_2-air premixed flame-wall interaction.
- In the stoichiometric H_2-air premixed flame case, the reactions $H_2+OH\rightarrow H_2O+H$ and $H_2+O\rightarrow OH+H$ can be sustained at relatively low temperatures if OH and O are supplied, and eventually, H is consumed in several intermediate chemical reactions (e.g. $O_2+H+M\rightarrow HO_2+M$, $H+O+M\leftrightarrow OH+M$, $H+OH+M\leftrightarrow H_2O+M$) which can take place at low temperature during the flame-wall interaction when O and OH diffuse to the near-wall region from the flame. These low-

temperature reactions lead to heat release rate at the wall for the head-on quenching of the stoichiometric H_2-air premixed flame.

- The differences in thermo-chemistry between stoichiometric hydrogen-air and methane-air premixed flames lead to considerable differences in the flame quenching distance and the maximum wall heat flux magnitude. The minimum Peclet number and the normalised wall heat flux magnitude are found smaller in the stoichiometric H_2-air premixed flame than in the stoichiometric CH_4-air premixed flame. Moreover, it has been found that the flame quenching distance tends to decrease under turbulent conditions for the head-on quenching of the stoichiometric H_2-air premixed flame but the quenching distances for laminar and turbulent conditions analysed here remain comparable for the stoichiometric CH_4 −air premixed flame.
- The FSD and SDR based mean reaction rate closures modified for capturing the near-wall behaviour using single-step chemistry DNS data in the past (Lai and Chakraborty, 2016a,b; Sellmann et al., 2017) have been found to perform reasonably well for the head-on quenching of both stoichiometric CH_4-air and H_2-air premixed flames.
- An algebraic SDR closure developed based on single-step chemistry DNS data has been found to perform well only for the head-on quenching of the stoichiometric CH_4-air premixed flame and its predictions are found to be inadequate in the near-wall region for the head-on quenching of premixed stoichiometric H_2-air premixed flames. Thus, it might be necessary to use the transport equation closures for modelling FSD and SDR in the case of head-on quenching of H_2-air premixed flames where the effects of differential diffusion of heat and mass can be significant.
- It may not be sufficient to model the mean reaction rate of major species to capture the mean heat release rate for the head-on quenching of the stoichiometric H_2 −air premixed flame because the mean reaction rate closure of the reaction progress variable based on major species mass fraction may not be sufficient to capture the important role played by intermediate species in the wall heat release in this case. Thus, further analyses will be needed for the closure of the mean heat release rate for the flame-wall interaction of premixed H_2 −air flames.

It is worth noting that the present analysis has been conducted for a single set of values of u'/S_L and l/δ_{th} but the statistics of wall heat flux, lame quenching distance and the performance of the mean reaction rate closure have been found to be valid for a wide range of turbulence intensities based on simple chemistry DNS (Lai et al., 2016a, Sellmann et al., 2017). Therefore, it can be expected that the conclusions drawn from this paper are not dependent only on one set of turbulent condition and are likely to remain quantitatively valid for a wide range of turbulent conditions. It is admitted that a change in equivalence ratio ϕ may modify some of the results presented here, as it changes the effective Lewis number of the flame. However, the stoichiometric cases considered here as a first attempt before analysing the equivalence ratio effects. Therefore, further investigation will be necessary to analyse effects of equivalence ratio on the comparison of HOQ characteristics between hydrogen-air and methane-air flames.

ACKNOWLEDGEMENTS

The authors are grateful to EPSRC (EP/R029369/1) for financial support and computational support from ARCHER, CSD-3, Leibniz Supercomputing Centre (grant: pn34xu) and ROCKET.

REFERENCES

Alshaalan, T. M. and Rutland, C. J., Turbulence, scalar transport, and reaction rates in flame-wall interaction. Proc. Combust. Inst., 27, 793-799 (1998).

Boger, M., Veynante, D., Boughanem, H., and Trouvé, A., Direct Numerical Simulation analysis of flame surface density concept for Large Eddy Simulation of turbulent premixed combustion, Proc. Combust. Inst., 27, 917-925 (1998).

Bray, K.N.C. 1980. Turbulent flows with premixed reactants. In Libby, P.A. and Williams, F.A. (eds.), Turbulent Reacting Flows, Springer Verlag, Berlin Heidelburg, New York, pp. 115-183.

Bruneaux, G., Akselvoll, K., Poinsot, T. and Ferziger, J. H., Flame-wall interaction simulations in a turbulent channel flow. Combust. Flame, 107, 27-44 (1996).

Bruneaux, G., Poinsot, T. and Ferziger, J. H., Premixed flame-wall interaction in a turbulent channel flow: budget for the flame surface density evolution equation and modelling. J. Fluid. Mech., 349, 191-219 (1997).

Cant, R.S. SENGA2 Manual, CUED-THERMO-2012/04, Cambridge University, 2nd Edition, Cambridge, UK (2012).

Chakraborty, N., Cant, R.S., Influence of Lewis Number on curvature effects in turbulent premixed flame propagation in the thin reaction zones regime, Phys. Fluids, 17,105105 (2005).

Chakraborty, N., Swaminathan, N., Effects of Lewis number on scalar variance transport in turbulent premixed flames, Flow Turb. Combust., 87, 261-292 (2011).

Dabireau, F., Cuenot, B., Vermorel, O. and Poinsot, T., Interaction of flames of H_2 -O_2 with inert walls. Combust. Flame, 135, 123-133 (2003).

Gruber, A., Sankaran, R., Hawkes, E.R., Chen, J.H., Turbulent flame-wall interaction: a direct numerical simulation study, J. Fluid Mech., 658, 5-32 (2010).

Jainski, C., Riβman, M., Böhm, B., Dreizler, A., Experimental investigation of flame surface density and mean reaction rate during flame–wall interaction, Proc. Combust. Inst., 36, 1827-1834 (2017a).

Jainski, C., Riβman, M., Böhm, B., Dreizler, A., Sidewall quenching of atmospheric laminar premixed flames studied by laser-based diagnostics, Combust. Flame, 183, 271-282 (2017b).

Jiang, B., Gordon, R.L. , Talei, M., Head-on quenching of laminar premixed flames diluted with hot products, Proc. Combust. Inst., 37, 5095-5103 (2019).

Jiang, B., Brouzet, D., Talei, M., Gordon, R.L., Cazeres, Q., Cuenot, B., Turbulent flame-wall interactions for flames diluted by hot combustion products, Combust. Flame, 230, 111432 (2021).

Kee, R. J et al., CHEMKIN Collection, Release 3.6, Reaction Design, Inc., San Diego, CA (2000).

Kosaka, H., Zentgraf, F., Scholtissek, A., Hasse, C., Dreizler, A., Effect of flame-wall interaction on local heat release of methane and DME combustion in a side-wall quenching geometry, Flow, Turb. Combust., 104,1029-1049 (2020).

Kolla, H., Rogerson, J.W., Chakraborty, N. and Swaminathan, N. Scalar dissipation rate modeling and its validation. Combust. Sci. Technol., 181, 518-535 (2009).

Konstantinou, I., Ahmed, U., Chakraborty, N., Effects of fuel Lewis number on the near-wall dynamics for statistically planar turbulent premixed flames impinging on inert cold walls, Combust. Sci. Technol., 193, 235-265 (2021).

Mann, M., Jainski, C., Euler, M., Böhm, B., Dreizler, A., Transient flame–wall interactions: Experimental analysis using spectroscopic temperature and CO concentration measurements, Combust. Flame, 161, 2371-2386 (2014).

Lai, J., Chakraborty, N., Effects of Lewis Number on head on quenching of turbulent premixed flame: A Direct Numerical Simulation analysis, Flow Turb. Combust., 96, 279-308 (2016a).

Lai, J., Chakraborty, N., Statistical behaviour of scalar dissipation rate for head on quenching of turbulent premixed flames: A Direct Numerical Simulation analysis, Combust. Sci. Technol., 188, 250-276 (2016b).

Lai, J., Chakraborty, N., A-priori Direct Numerical Simulation modelling of scalar dissipation rate transport in head-on quenching of turbulent premixed flames, Combust. Sci. Technol., 188,1440-1471 (2016c).

Lai, J., Moody, A., Chakraborty, N., Turbulent kinetic energy transport in head-on quenching of turbulent premixed flames in the context of Reynolds Averaged Navier Stokes simulations, Fuel, 199, 456-477 (2017a).

Lai, J., Chakraborty, N., Lipatnikov, A., Vorticity and enstrophy transport in head-on quenching of turbulent premixed flames, Eur. J. Mech. Fluids/B, 65, 384-397 (2017b).

Lai, J., Alwazzan, D., Chakraborty, N., Turbulent scalar flux transport in head-on quenching of turbulent premixed flames in the context of Reynolds Averaged Navier Stokes simulations, J. Turb., 188, 11 (2017c).

Lai, J., Chakraborty, N., Direct Numerical Simulation of head-on quenching of statistically planar turbulent premixed methane-air flames using a detailed chemical mechanism, Flow, Turb. Combust.,101, 1073-1091 (2018).

Li, J., Zhao, Z., Kazakov, A., Chaos, M., Dryer, F., Scire Sr., S, A comprehensive kinetic mechanism for CO, CH2O, and CH3OH combustion, Int J Chem Kinet, 36, 565 (2004).

Liu, F., Guo, H., Smallwood, G.J., Gulder, O.L., Numerical study of the superadiabatic flame temperature phenomenon in hydrocarbon premixed flames, Prof. Combust. Inst., 29, 1543 (2002).

Palulli, R., Talei, M., Gordon, R.L., Unsteady flame–wall interaction: Impact on CO emission and wall heat flux, Combust. Flame, 207, 406-416 (2019).

Peters, N., Turbulent Combustion, Cambridge Monograph on Mechanics, Cambridge University Press, Cambridge (2000).

Poinsot, T., Veynante, D., Theoretical and numerical combustion, R.T. Edwards Inc., Philadelphia, USA (2001).

Poinsot, T., Lele, S.K., Boundary conditions for direct simulation of compressible viscous flows, J. Comp. Phys., 101, 104-129 (1992).

Poinsot, T., Haworth, D.C., Brauneaux, G., Direct simulation and modelling of flame-wall interaction for premixed turbulent combustion, Combust. Flame, 95, 118-132 (1993).

Rogallo, R.S., Numerical experiments in homogeneous turbulence, NASA Technical Memorandum 81315, NASA Ames Research Center, California (1981).

Rutland, C., and Trouvé, A., Direct Simulations of premixed turbulent flames with nonunity Lewis numbers, Combust. Flame, 94, 41-57 (1993).

Sellmann, J., Lai, J., Chakraborty, N., Kempf, A.M., Flame Surface Density based modelling of head-on quenching of turbulent premixed flames, Proc. Combust. Inst., 36, 1817-1825 (2017).

Smooke, M.D., Giovangigli, V., Premixed and nonpremixed test flame results, in Reduced kinetic mechanisms and asymptotic approximations for methane-air flames, Springer, Berlin, pp. 29-47 (1991).

Strategic framework for hydrogen energy in the UK (2004) http://berr.gov.uk/files/file26737.pdf.

Veynante, D., Trouvé, A., Bray, K.N.C., Mantel, T., Gradient and counter-gradient scalar transport in turbulent premixed flames, J. Fluid Mech., 332, 263-293 (1997).

Zhang, S., Rutland, C.J., Premixed flame effects on turbulence and pressure related terms, Combust. Flame 102, 447-461 (1995).

Zhao, P., Wang, L., Chakraborty, N., Analysis of the flame-wall interaction in premixed turbulent combustion, *J. Fluid Mech*., 848, 193-218 (2018).